DYNAMICS OF THE LARGE-SCALE STRUCTURES OVER A STREET CANYON IN AN URBAN-TYPE BOUNDARY LAYER

Laurent Perret
Laboratoire de Mécanique des Fluides,
Ecole Centrale de Nantes, UMR CNRS 6598
1 rue de la Noë BP 92101, F-44321 Nantes Cedex 3, France
laurent.perret@ec-nantes.fr

Eric Savory
Department of Mechanical & Materials Engineering
University of Western Ontario
London, ON N6A 5B9, Canada
esavory@eng.uwo.ca

ABSTRACT

Wind tunnel PIV experiments were performed in order to investigate the dynamics of the large-scale structures over a street canyon model which consists of two parallel obstacles placed perpendicular to the main flow. The oncoming flow was an urban-type boundary layer developing over roughness elements the height of which was more than ten percent of the boundary layer depth. Attention was concentrated on the dynamics of the shear layer emanating from the top of the upstream obstacle and the occurrence of unsteady penetration and ejection of fluid from the canyon. The investigation of the structure of the shear layer region was performed via the analysis of two-point spatial correlations and the use of Proper Orthogonal Decomposition and conditional averaging techniques. It was found that the shear layer separating from the upstream obstacle was animated by a coherent flapping motion and generated large-scale vortical structures. These structures were alternatively injected into the canyon or shed off the obstacle downstream in the outer flow. Unsteady fluid exchanges between the canyon cavity and the outer flow were found to be mainly driven by the shear layer separating from the upstream obstacle.

INTRODUCTION

In an environmental context, flow over and inside cavity-like geometries such as urban canyons are of great interest because of the transport processes (of air, pollutants, aerosols, etc) that occur between the cavity and the main flow above. The steady organization of the canyon flow, consisting of a single vortex in the case of a square-section canyon, the axis of which is perpendicular to the main flow, is now well-known. However, understanding the dynamics of this type of flow is crucial when dealing with environmental applications such as the prediction of the concentration level and the spreading of an accidentally released pollutant. Even if there exist some geometrical similarities between urban canyons and 2D cavities encountered in other engineering applications, the flow separation at the upstream edge of the upstream obstacle and the nature of the oncoming urban boundary layer may induce some strong differences in the flow dynamics. The dynamics of the flow inside and at the top of a 2D cavity has indeed been shown to be strongly influenced by the level of upstream turbulence (Chang *et al.*, 2006; Haigermoser *et al.*, 2008; Kang & Sung, 2009). In particular, the ratio between the depth of the cavity and the momentum thickness of the upcoming boundary layer has been found to be a key parameter in the dynamics of the shear layer at the top of the cavity (Kang & Sung, 2009). In the case of the urban canyon, the typical scale of the coherent structures of the oncoming boundary layer are larger than the depth of the canyon (Castro *et al.*, 2006) and so the dynamics of the flow are expected to be quite different. The review by Jimenez (2004) devoted to boundary layer flows over roughened walls, showed that the roughness Reynolds number and the ratio of the boundary layer thickness to the roughness height were two important parameters which measure the interference of the roughness with the buffer layer and the logarithmic layer, respectively. In addition, a distinction has been made between k-type roughness flow where wakes and separation bubbles are fully developed and d-type roughness flow over which the flow skims. Recent studies on flows over two-dimensional k-type roughness (Lee *et al.*, 2008; Cardwell *et al.*, 2011) focused on vortex structures induced by the rod-roughness elements and the fluid motion in the near-wall region, providing evidence of the relationships between vortices induced by shedding from the rod and sweeping or bursting events.

The present work is an experimental study of the turbulent flow within and above an urban canyon, whose main goal is to quantify the dynamics of the shear layer emanating from the top of the upstream obstacle and the occurrence of unsteady penetration and ejection of fluid inside the canyon.

EXPERIMENTAL DETAILS

In this section, a description of the experimental apparatus and procedures and details of the generated urban boundary layer are provided

Experimental setup

Experiments were conducted in the atmospheric boundary layer wind tunnel of the Laboratoire de Mécanique des Fluides (Nantes, France), which has working section dimensions of $24 \times 2 \times 2$ m. A simulation of a suburban-type atmospheric boundary layer was achieved at the test model location by using three vertical, tapered spires over the entire height of the inlet of the working section, a 300mm high solid fence across the working section located 1.5m downstream of the inlet, followed by an 18.5m fetch of staggered cube roughness elements with a plan area density of 6.25%. The cube height was $H = 0.1$m. The plan area density of the roughness elements corresponds to a k-type rough wall. The boundary layer mean velocity and turbulence profiles were measured using a crossed hot-wire anemometry system. The measurements were performed with a free stream velocity, U_e, of 5.9 ms^{-1}. Characteristics of the generated boundary layer are described in detail in the following section. The canyon model consisted of two square-section rectangular blocks, placed perpendicular to the flow, whose height was H and length $L/H = 14$, with a spacing, representing the street width, of $W/H = 1$ (figure 1).

Two-component PIV measurements were conducted in a vertical plane aligned with the main flow, in the centre of the canyon. Two sets of 2,000 velocity fields were recorded (with a sampling frenquency of 1Hz) to enable the computation of the main flow statistics and investigate its large-scale organization in and above the canyon (figure 1). The first set spanned the width of the canyon, over a height of $1.6H$. A 1344×1024 pixels 12 bits CCD camera equipped with a 60mm objective lens was employed to investigate this region. The final spatial resolution of the vector field was 2mm (0.02H). The second set covered the region $-1.5 \leq x/H \leq 0.5$ and $1 \leq z/H \leq 3$ above the upstream obstacle and the canyon. A 2000×2000 pixels 12 bits camera equipped with a 105mm objective lens was employed. This setup gave a final spatial resolution of 1.55mm (0.015H). A 50 mJ Nd-Yag laser was used to illuminate one or the other region. The flow was seeded with glycol/water droplets (typical size 1mm) using a fog generator. The synchronisation between the laser and the camera and the calculation of the PIV velocity vector fields were performed using the DANTEC FlowManager software.

The FFT-based 2D-PIV algorithm with sub-pixel refinement was employed. Iterative cross-correlation analysis was performed with initial window size of 64×64 pixels and with 32×32 final interrogation windows. An analysis window overlap of 50% was used. Spurious vectors were detected by an automatic validation procedure whereby the SNR of the correlation peak had to exceed a minimum value, and the vector amplitude had to be within a certain range of the local median to be considered as valid. Once spurious vectors had been detected, they were replaced by vectors resulting from a linear interpolation in each direction from the surrounding 3×3 set of vectors. Velocity gradients were computed by using a second-order centred difference scheme.

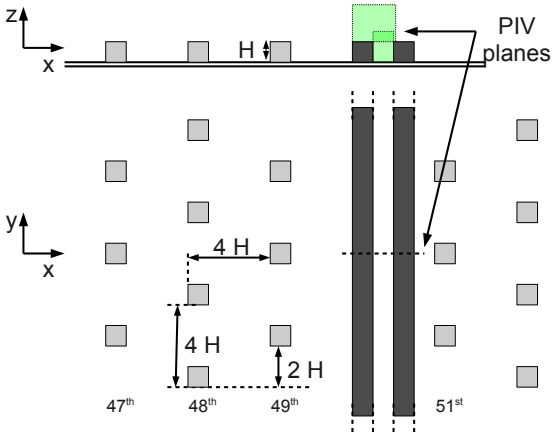

Figure 1. Experimental setup.

Table 1. Characteristics of the upstream boundary layer

H^+	u^*/U_∞	δ/H	d/H	z_0/H
2300	0.058	11.6	0.548	0.022

Upcoming boundary layer

As the present study was performed in the framework of urban-like flows, some efforts were devoted to the simulation of a boundary layer with roughness length z_0 and displacement height d characteristics of suburban terrain. These parameters are used in the usual meteorologists' version of the log-law profile to describe the evolution of the mean longitudinal velocity profile:

$$\frac{U}{u^*} = \frac{1}{\kappa} ln\left(\frac{z-d}{z_0}\right) \quad (1)$$

where u^* is the friction velocity derived from the wall-shear stress, z the distance from the wall and $\kappa = 0.41$ the Kármán constant. The 99% thickness of the obtained boundary layer was $\delta = 1.16m$. The measured profile of the mean streamwise velocity clearly exhibits a logarithmic region that extends over almost $2H$ (figure 2, top). The value of u^* was derived from the constant shear stress region exhibited by the flow (figure 2, bottom). These two profiles were used to find the above defined roughness parameters that are summarized in table 1. The values of δ/H and of the non-dimensional obstacle height $H^+ = Hu^*/\nu$ indicate that the effect of the roughness elements will extend far from the wall, making the flow aerodynamically fully rough, consistently with the behaviour of atmospheric flows (Jimenez, 2004). This characteristic is also confirmed by the shape of the profiles and the maximum value of the variance of the streamwise and wall-normal fluctuations (figure 2, bottom). Values of d/H and z_0/H also correspond to flow developing over urban terrain with low building density (Grimmond & Oke, 1999).

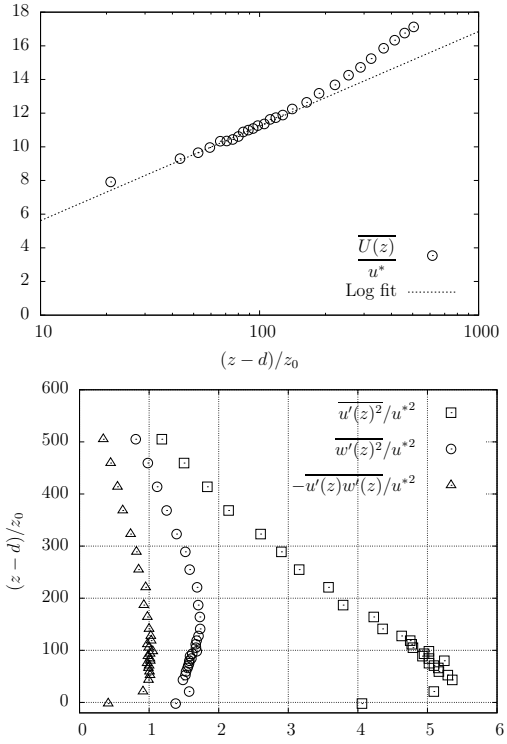

Figure 2. Profiles of the mean streamwise velocity (top) and turbulent quantities (bottom) measured in the upstream boundary layer.

RESULTS

In this section, both the statistical characteristics and the large-scale dynamics of the flow over and within the canyon are investigated, based on the PIV database.

One-point statistics

Iso-contours of the mean velocity (figure 3a and b) are consistent with the presence of a vortex core inside the canyon, the diameter of which being of the order of the height and width of the cavity. These velocity maps also show the presence of a strong shear layer originating from the top of the upstream obstacle, corresponding to the location of the maximum vertical gradient of the mean longitudinal velocity. The two-dimensional turbulent kinetic energy $\mathrm{TKE}^{(2d)}$, evaluated from the two in-plane components and defined as $\mathrm{TKE}^{(2d)} = 0.5(\overline{u'^2} + \overline{w'^2})$, is also maximum in this region and corresponds to a region of high shear $-\overline{u'w'}$ (figures 3c and d). Separation of the upstream flow from the sharp corner of the upstream building generates a strong shear layer, similar to that existing in flow over a *k*-type rod-roughened wall (Cardwell *et al.*, 2011) in which the flow can reattach between two rods. However, here, the presence of the downstream obstacle greatly reduces the penetration of the flow within the canyon, corresponding more to a skimming flow regime or flow over *d*-type roughness. Moreover, inspection of instantaneous velocity fields showed that this shear layer presents a vertical flapping motion that seems to induce penetrations or ejections of fluid within the canyon combined with large-scale vortices shed from the upstream obstacle that are convected downstream in the boundary layer.

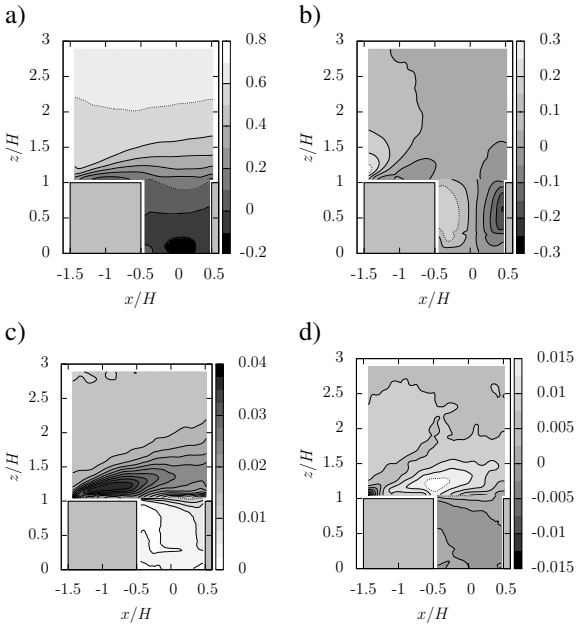

Figure 3. One-point statistics of the flow obtained from PIV measurements. a): $\overline{u}/U_e$, b): $\overline{w}/U_e$, c): $\mathrm{TKE}^{(2d)}/\mathrm{U_e}^2$, d): $-\overline{u'w'}/{U_e}^2$

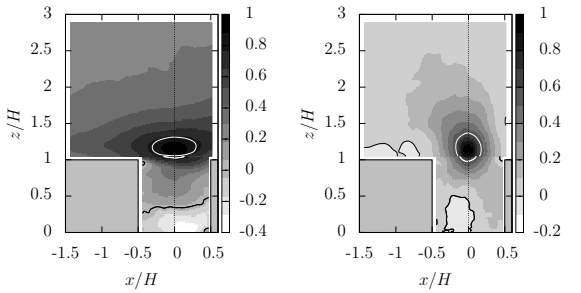

Figure 4. Two-point correlation maps obtained for a reference located at $x_{ref}/H = 0$, $y_{ref}/H = 1.2$. Left: $R_{uu}(x_{ref}, y_{ref}, x, y)$, right: $R_{ww}(x_{ref}, y_{ref}, x, y)$. Black solid line, zero-contour level, white solid line, level used for ellipse fitting.

Two-point statistics

Investigation of the flow exchange between the canyon and the flow above is studied here via the computation of the two-point coefficient correlation of both the streamwise and the vertical velocity components. These quantities are defined as:

$$R_{uu}(x_{ref}, y_{ref}, x, y) = \frac{\overline{u'(x_{ref}, y_{ref}) u'(x, y)}}{\sqrt{\overline{u'^2(x_{ref}, y_{ref})}}\sqrt{\overline{u'^2(x, y)}}} \qquad (2)$$

where (x_{ref}, y_{ref}) are the coordinates of the fixed point. Correlations of the vertical component *w* are computed in a similar way. Computation of the correlations within the canyon

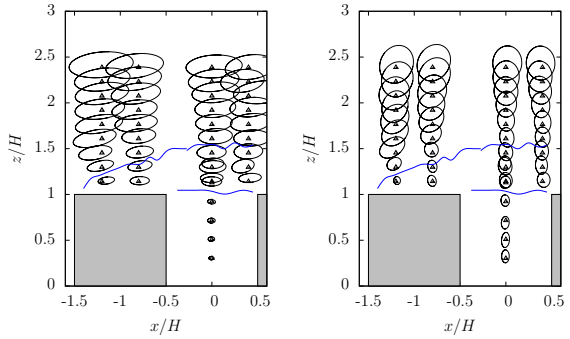

Figure 5. Shape of the two-point correlation obtained for different locations of the reference point. Left: R_{uu}, right: R_{ww}. For clarity, ellipses are drawn half of their actual size. Solid line: shear layer boundaries.

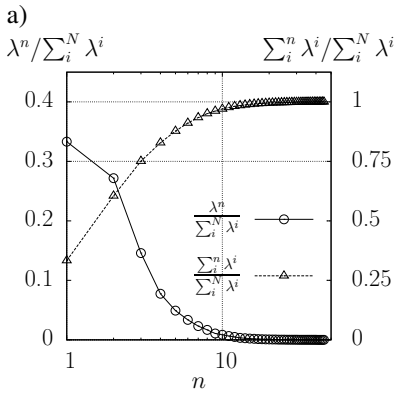

Figure 6. Energy contribution of POD eigenvalues λ^n.

(not shown here), shows that this region seems to be decoupled from the shear layer and the flow above the shear layer, in agreement with the skimming flow regime. Figure 4 shows an example of correlation maps obtained in the shear layer region ($z_{ref}/H = 1.2$), on the centreline of the canyon. Both R_{uu} and R_{ww} are mainly positive but also exhibit negative levels (black solid lines on figure 4 correspond to a correlation level of zero) inside the canyon, which is consistent with the clockwise recirculation motion in this region. In addition, R_{ww} shows negative levels above the upstream obstacle, which can be interpreted as being the footprint of large scale vortical structures developing inside the shear layer emanating from the upstream corner of the upstream building. The origin of the shear layer is the main difference existing between cavity flow configurations where the shear layer starts from the downstream corner (Kang & Sung, 2009) and the present configuration. This is confirmed by the investigation of the correlations near the top of the obstacles (not shown here) that indicates that, contrary to many canonical cavity flows (Kang & Sung, 2009), large-scale vertical motion of fluid exists in this region rather than well organized vortex shedding. Correlations computed above the shear layer have a shape and length scales in agreement with that existing in flows developing above urban-like roughness (Coceal *et al.*, 2007*b*). These characteristics are not addressed in the present study and the focus is put on the organization of the shear layer region.

From the above analysis, it appears that correlation maps have two distinct features: their shapes and their inclinations. R_{uu} is more elongated in the streamwise direction and exhibits a preferential inclination; R_{ww} tends to be more isotropic, with shorter length scales. To quantify the variation of these characteristics with the location within the flow, ellipses were fitted to a given contour extracted from R_{uu} and R_{ww} calculated for different values of x_{ref} and y_{ref}. Given the limited extent of the PIV field of view, rather high values of correlation contours were used here, in comparison to the more common value of 0.4 (Coceal *et al.*, 2007*b*). Even if this leads to an underestimation of the typical length scales of the flow, the shapes and inclinations are well estimated and allow for a qualitative analysis of the flow structure. Figure 5 shows the result of this analysis. Ellipses are drawn half of their actual size for clarity. The solid lines correspond to the limits of the shear layers developing from the upstream obstacle, which were identified from the local maxima of the $\mathrm{TKE}^{(2d)}$ gradient, $\partial \mathrm{TKE}^{(2d)}/\partial z$ (Cardwell *et al.*, 2011). In addition to the conclusions that were drawn above, it is noticeable that, in the shear layer region, the inclination and the length scales of R_{uu}, respectively, decrease and increase with the longitudinal distance from the upstream edge of the upstream obstacle, following the growth of the shear layer. Within the shear layer, at a given streamwise location, length scales are constant with height. Above the shear layer, the characteristic length scales of the correlation appear to progressively increase with height, in accordance with the evolution of length scales in a boundary layer over large roughnesses (Coceal *et al.*, 2007*b*). It confirms that, on average, three distinct regions exists, delimited by the shear layers emanating from the edges of the upstream building and characterized by different length scales and orientation of the structures.

Organization of coherent structures

In order to investigate the flow transfer processes across the canyon opening that may be induced by the large scale motion existing in the flapping shear layer, the dynamics of the vertical component w at $z/H = 1$ is studied through the use of the Proper Orthogonal Decomposition (POD) (Lumley, 1967). Based on the quantity $R_{ww}(x,x',z=H)$, a one-dimensional POD analysis was performed to decompose the vertical velocity component into a set of spatial and temporal eigenmodes $\phi_w^n(x)$ and $a_n(t)$, respectively, such that:

$$w(x,t) = \sum_{n=1}^{N} a_n(t)\phi_w^n(x). \qquad (3)$$

The spatial modes $\phi_w^n(x)$ form an orthonormal basis of the flow and the temporal coefficients $a_n(t)$ represent the dynamics of the corresponding modes. The eigenvalue λ^n represents the energy contribution of the n^{th} mode to the total turbulent energy.

The energy content of the first two POD modes, given by the first two eigenvalues (figure 6), is found to represent more than 60% of the total turbulent energy associated with the vertical fluctuations. The spatial shape of these two modes (figure 7, left) corresponds to strong penetration or ejection motions through the opening of the canyon. Analysis of the higher order modes (not shown here) did not give any information on

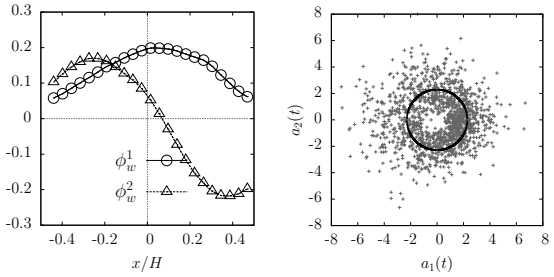

Figure 7. First two POD modes $\phi_w^1(x)$ and $\phi_w^2(x)$ (left) and phase portrait of POD coefficients $a_1(t)$ and $a_2(t)$ (right).

the possible existence of organized vortex shedding (e.g. very similar spatial modes with a phase difference of a quarter of the pseudo period). These two most energetic modes are also found to contain most of the energy during 70% of the time (e.g. the maximum mode amplitude is either $a_1(t)$ or $a_2(t)$, 70% of the time), meaning that the dynamics of the flow is mostly driven by these two modes. The phase portrait of the time-varying coefficients $a_1(t)$ and $a_2(t)$ when either $a_1(t)$ or $a_2(t)$ is maximum reveals that they are more or less located around a circle (figure 7, right). This means that a strong dynamical relationships exists between these two modes and confirms the temporal coherence of the penetration and ejection motions directly observed on the instantaneous velocity fields. This particular distribution also allows the computation of a phase angle between $a_1(t)$ and $a_2(t)$ defined by

$$\alpha_{a_1-a_2} = \arctan\left(\sqrt{\frac{\lambda^1}{\lambda^2}}\frac{a_2(t)}{a_1(t)}\right). \qquad (4)$$

Phase averaged velocity fields are then computed by averaging instantaneous velocity fields which correspond to the instantaneous angle $\alpha_{a_1-a_2}$ falling into a given range. The whole range of possible angles $[0, 2\pi]$ was divided into 18 sub-intervals. Analysis of the 18 phase averaged velocity fields shows that a strong flapping of the flow exists above the canyon, which corresponds to penetration (figure 8a and b) and ejection (figure 8c and d) of fluid through the canyon opening. In order to investigate further the organisation of the flow, vortical structures, identified by a positive value of the swirling strength λ_{ci} are extracted from the instantaneous velocity fields and phase averaged. The swirling strength, computed from the imaginary part of the complex conjugate eigenvalues of the local velocity gradient tensor, has been shown to be frame-independent and able to discriminate compact vortical cores from regions of intense shear (Chakraborty *et al.*, 2005). Phase averaged λ_{ci} distributions show that the vertical fluid motions throughout the canyon opening are accompanied by vortical structures (figure 8).

Based on the occurrence of ejection (Q2) or penetration (Q4) events, conditionally averaged velocity field and swirling strength signed by the vorticity sign λ_{ci}^s were computed from the PIV database measured above the canyon. This analysis was performed independently of the above as the two PIV experiments were completely decorrelated. Q2 or Q4 events occurring in the shear layer region, along the canyon centreline (figures 9, top and bottom, respectively), turned out to

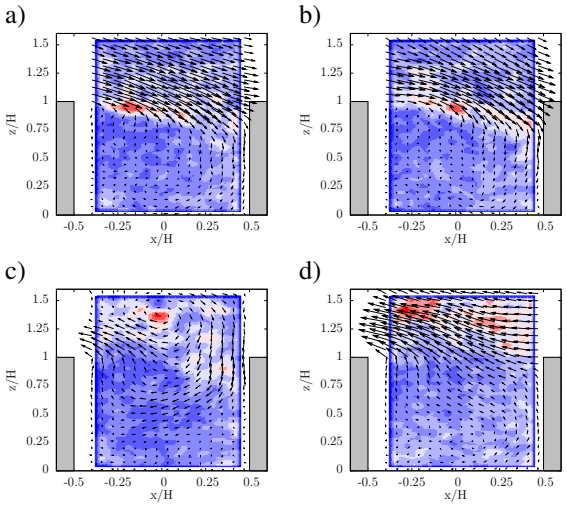

Figure 8. Examples of phase averaged velocity fields (1 every 3 vector shown) corresponding to, a) and b), penetration of fluid and, c) and d), ejection of fluid. The mean velocity field has been substracted for more clarity. Contours: level of phase-averaged swirling strength λ_{ci}; blue corresponds to zero level, red to high value of λ_{ci}.

be strongly correlated to a clockwise rotating vortical motion ($\lambda_{ci}^s < 0$) existing in the shear layer above the top of the obstacles, in agreement with the previous POD analysis. The flapping motion of the shear layer is also clearly evidenced here. Figure 9, top, also suggests that the vortical structures associated with strong Q2 events in the shear layer are convected downstream and may participate to the generation of vortical structures populating the boundary layer.

When based on a Q2 or Q4 event occurring well above the shear layer, the conditionally-averaged swirling strength distribution is found to be almost independent of the nature of the conditional event, meaning that the dynamics of the flow just above the canyon is primarily driven by the shear layer dynamics separating from the upstream building.

CONCLUSIONS

A wind tunnel experiment has been performed to investigate the dynamics of the turbulent large-scale structures that develop above and within a street canyon model that is embedded in an urban-like atmospheric boundary layer. The experimental configuration is based on a street canyon model, of equal height and streamwise width, and the generation of a boundary layer over roughness elements with a plan area density of 6.25%. This can be viewed as being equivalent to the combination of a localized d-type roughness within a k-type flow with low δ/H ratio. A strong influence of the roughness on the flow dynamics is then expected and observed in the present case. Analysis of the PIV database via the computation of two-point spatial correlations and the use of Proper Orthogonal Decomposition and conditional averaging techniques shows that the flow dynamics are different from canonical cavity flows. The k-type regime of the flow upstream of the canyon indeed leads to a strong separation of the flow from the upstream obstacle, leading, in turn, to the

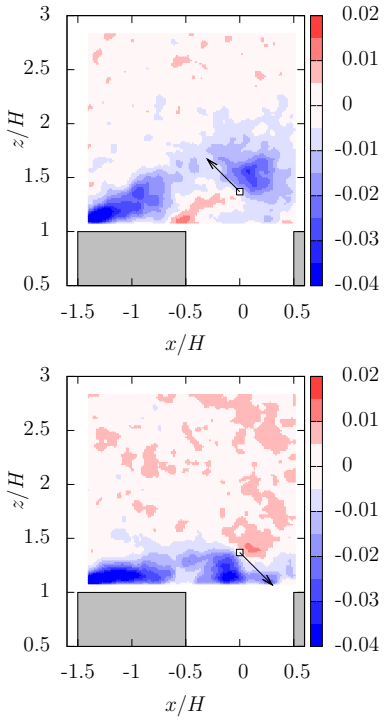

Figure 9. Conditional average of the signed swirling strength distribution λ_{ci}^{s} based on, top, a Q2 event and, bottom, a Q4 event, occurring at $x/H = 0$, $z/H = 1.37$.

formation of a shear layer. This shear layer develops over the top of the two obstacles and the canyon, and generates, as in a more classical mixing layer, vortical structures of spanwise vorticity, the length scale of which increases with downstream distance. In addition, the shear layer region is animated by a flapping motion that is found to be responsible for the unsteady flow exchanges between the canyon and the outer flow. These exchanges consist of penetration or ejection of fluid from the canyon, which are combined with vortical structures that penetrate into the canyon or are shed and convected in the outer flow, respectively. The strong Q2 and Q4 events observed above the canyon opening, that extend up to $z = 2H$, are strongly correlated to the shear layer. In the present case, these events should be qualified more as 'penetration' and 'flushing' events rather than the 'sweeps' and 'ejections' related to the hairpin vortex packet model. Analysis of the two-point correlations also revealed that the presence of the shear layer tends to decouple the flow within the canyon from the dynamics of the upstream boundary layer. However, this point is still subject to interrogations and remains open. The results obtained are in agreement with the conceptual model derived by Coceal *et al.* (2007*a*) by DNS in the case of a boundary layer flow developing over an array of 3-dimensional obstacles. The main differences are believed to be due to the two-dimensional character of the canyon investigated here and its local *d*-type flow regime.

The present findings lead to several remaining questions regarding the dynamics of the shear layer and its separation mechanism, including links with the dynamics of the coherent structures of the upstream boundary layer. Attention should also be given to the effect of the canyon geometry (height to width ratio or length to height) on the unsteady exchange of fluid between the canyon and the outer flow. Several studies have already been devoted to the investigation of the influence of these geometrical parameters on the mean flow structure, but the flow dynamics remains to be studied.

ACKNOWLEDGEMENTS

Dr Savory's sabbatical at Ecole Centrale de Nantes (France) was supported by the Regional Council of the Pays de La Loire (France). This work was also supported by the Regional Council of the Pays de La Loire within the framework of the project EM2PAU.

REFERENCES

Cardwell, N D, Vlachos, P P & Thole, K A 2011 Developing and fully developed turbulent flow in ribbed channels. *Experiments in Fluids* **50**, 13571371.

Castro, I P, Cheng, H & Reynolds, R 2006 Turbulence over urban-type roughness: deductions from wind-tunnel measurements. *Boundary-Layer Meteorology* **118**, 109–131.

Chakraborty, P, Balachandar, S & Adrian, R J 2005 On the relationships between local vortex identification schemes. *Journal of Fluids Mechanics* **535**, 189–214.

Chang, K, Constantinescu, G & Park, S 2006 Analysis of the flow and mass transfer processes for the incompressible flow past an open cavity with a laminar and a fully turbulent incoming boundary layer. *Journal of Fluids Mechanics* **561**, 113–145.

Coceal, O, Dobre, A & Thomas, T G 2007*a* Unsteady dynamics and organized structures from DNS over an idealized building canopy. *International Journal of Climatology* **27**, 1943–1953.

Coceal, O, Dobre, A, Thomas, T G & Belcher, S E 2007*b* Structure of turbulent flow over regular arrays of cubical roughness. *Journal of Fluids Mechanics* **589**, 375–409.

Grimmond, C S B & Oke, T R 1999 Aerodynamic properties of urban areas derived from analysis of surface form. *Journal of Applied Meteorology* **38**, 1262–1292.

Haigermoser, C, Vesely, L, Novara, M & Onorato, M 2008 A time-resolved particle image velocimetry investigation of a cavity flow with a thick incoming turbulent boundary layer. *Physics of Fluids* **20**, 1–14.

Jimenez, J 2004 Turbulent flows over rough walls. *Annual Review of Fluids Mechanics* **36**, 173–196.

Kang, W & Sung, H J 2009 Large-scale structures of turbulent flows over an open cavity. *Journal of Fluids and Structures* **25**, 1318–1333.

Lee, S-H, Kim, J H & Sung, H J 2008 PIV measurements of turbulent boundary layer over a rod-roughened wall. *International Journal of Heat and Fluid Flow* **29**, 1679–1687.

Lumley, J L 1967 *The structure of inhomogeneous turbulence*. Atmosphere, Turbulence and Radio Wave Propagation. Nauka, Moscow.